

Towards Meshless Methods for Surgical Simulation

Ashley Horton, Adam Wittek, Karol Miller

Intelligent Systems for Medicine Laboratory
School of Mechanical Engineering, The University of Western Australia
35 Stirling Highway, Crawley, Perth WA 6009 Australia
{ahorton, adwit, kmiller}@mech.uwa.edu.au

Abstract. For the purpose of surgical simulation, we propose an algorithm based upon the Element Free Galerkin method, Total Lagrangian explicit dynamics and nonlinear material formulation. The proposed algorithm does not require a finite element mesh, so is well suited to simulations with irregular geometry. As an example, a simplified 3D simulation of craniotomy induced brain shift including brain, ventricles, tumor, subarachnoid space and skull is performed. The algorithm is validated by comparing simulation results with a well established commercial code.

Keywords: Element Free Galerkin, Total Lagrangian, brain shift

1 Introduction

In recent years efforts to calculate soft tissue deformation for surgical simulations have typically been based on Finite Element Analysis (FEA) [1-3]. The results from these FEA experiments have been promising, showing that near real-time simulations of surgical procedures, using nonlinear (both geometric and material) biomechanical models, can be achieved with a high level of precision [3-5]. Accuracy in the FEA calculation relies heavily on the element mesh which discretises the geometry in question and often we wish to use only hexahedral elements. When the geometry is highly irregular, an experienced analyst is required to manually create such a mesh which consumes valuable time. This is a major bottleneck; efficient generation of models to be used in real-time simulation of surgical procedures.

One solution to this bottleneck is to use a numerical method that does not have such strict discretisation requirements. In [6] we proposed the use of the Element Free Galerkin method (EFG) [7] which uses a cloud of unconnected nodes to discretise the geometry instead of elements. Placement of these nodes can be done automatically since their arrangement is almost arbitrary.

Further advantages of using EFG for neurosurgical procedures include its ability to deal with large deformation and topology changes [8] that occur during procedures such as retractions and cuts. These areas are not covered in the present study but should be kept in mind as an advantage of EFG.

In [6], we simulated craniotomy induced brain shift with both EFG and FEA in LS DYNA [9]. Although slightly slower, EFG gave very similar results to FEA and can certainly be considered for use in future simulations. The major limitation of LS DYNA's implementation of EFG is the fact that it requires a complete mesh of hexahedral elements that conform to the geometry exactly. By employing this mesh of hexahedral elements, LS DYNA ensures that nodes are evenly distributed through the problem domain which reduces the possibility of near singular shape functions (see section 2.1). Background integration is also performed over these elements so the volume of integration matches the volume of the problem's geometry perfectly. However, requiring this structured hexahedral mesh, removes the method's ability to deal with irregular geometries easily.

An algorithm that does not require a geometry conforming hexahedral element mesh is a necessary step towards using meshless methods for fast, efficient simulation of surgical procedures.

2 The Proposed Algorithm

We now give a brief description of our algorithm with reference to the neurosurgical example discussed in sections 3 and 4.

2.1 The Element Free Galerkin Method

The main idea of EFG, is the creation of shape functions from a cloud of unconnected nodes. For any point x^* in the problem domain, we consider a compact region D on x^* and observe the n nodes within D . The Moving Least Squares approximant [10] of the field variable $u(x)$ on D is

$$u^h(x) = p^T(x)a(x) \quad (1)$$

Where $p(x)$ is a monomial basis vector of order $m < n$ and $a(x)$ is the coefficient vector that minimises the functional shown in (2).

$$J = \sum_{i=1}^n W(d_i)(p^T(x_i)a(x) - u(x_i))^2 \quad (2)$$

$W: \mathbb{R} \rightarrow \mathbb{R}$ is a weight function and d_i is the distance between the node x_i and x^* .

In both neurosurgical simulations described in this paper, we use monomial basis functions up to quadratic order. However, because we only use a thin slice of volume (see section 3.1) there are insufficient points to create unique shape functions in 3D. In our example, some higher order monomial basis functions were removed in the direction normal to the slice (ie, if z is normal to the slice, then the terms xz , yz and z^2 have been removed).

2.2 Total Lagrangian Explicit Dynamics

Where LS DYNA uses Updated Lagrangian (UL) formulation, our algorithm uses Total Lagrangian (TL). The difference between these methods is that in UL, the calculated variables are referred to the previous calculated configuration, as opposed to the initial configuration for TL [2]. As in [11], our method precomputes the constant strain-displacement matrices for each integration cell and uses the deformation gradient to calculate the full matrix at each time step.

Both LS DYNA and our algorithm use explicit time integration, based on the central difference method [2].

2.3 Material Properties

In the example given in section 3, there are three parts that require modeling of material properties, the brain, ventricles and tumor. For the brain and tumor, we use the simplest fully nonlinear material formulation, Neo-Hookean [2]. We are justified in using the simplest possible nonlinear form because at this point we are primarily interested in comparing our numerical algorithm to LS DYNA's.

The Neo-Hookean formulation is obtained by simplifying the Mooney-Rivlin [2, 12] rubber model used in LS DYNA. According to [9], Mooney-Rivlin rubber in LS DYNA has the strain energy density function

$$W = A(I - 3) + B(II - 3) + C(III^{-2} - 1) + D(III - 1)^2 \quad (3)$$

where A , B and ν are parameters and

$$C = \frac{A}{2} + B$$

$$D = \frac{A(5\nu - 2) + B(11\nu - 5)}{2(1 - 2\nu)}.$$

I , II and III are the first, second and third invariants of the right Cauchy-Green deformation tensor.

The parameters we use for healthy brain tissue are $A=1052$ Pa, $B=0$ Pa and $\nu=0.49$. Note that by setting $B=0$ we are simplifying the model to almost incompressible Neo-Hookean since ν is Poisson's ratio. The value for A is derived from [13, 14]. For the tumor, we use the same justification as [3] to assume the properties of healthy brain.

We model the ventricles as soft, compressible elastic solids with Young's modulus 10Pa and Poisson's ratio of 0.1. Justification for this is given in [3].

3 Neurosurgical Example

The following example is given to show how our algorithm can be used in the place of LS DYNA's existing code. The example is a simple one, but contains all the major components (3D, finite deformation, nonlinear material models, irregular geometry, multiple parts and contact definitions) of a more complicated simulation. Parallel simulations are run in both LS DYNA and with our algorithm.

3.1 Base Images and Geometry

The geometry for our patient-specific, brain shift simulation is based on pre-operative MRIs (Fig. 1) segmented with 3D Slicer [15] by the Surgical Planning Laboratory at Brigham and Women's Hospital and Harvard Medical School.

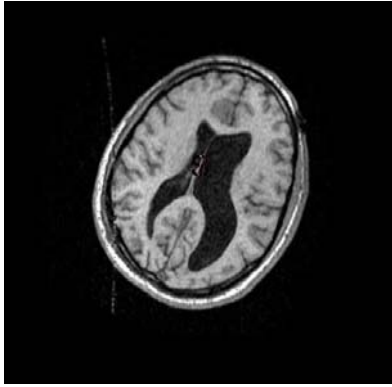


Fig. 1. Patient specific data. MRI showing ventricles (dark centre), brain and skull. A tumor is present, but experience and skill are required to accurately differentiate it from healthy brain tissue.



Fig. 2. Segmented MRI clearly showing ventricles, brain, skull and tumor.

We choose our experimental geometry to be a thin, 3D slice of brain obtained by taking the 2D segmented image shown in Fig. 2, and applying a uniform thickness of 5mm using the Ansys pre-processor [16]. Complete justification for this is given in [6], but the main point to note is that full 3D formulations are employed throughout this study.

3.2 Discretising the Geometry

For the LS DYNA simulation, we use the same node arrangement and hexahedral element used in [6]. Integration is done over the hexahedral elements shown in Fig.3.

Unlike LS DYNA, our algorithm can take randomly placed nodes. However, a truly random placement is often not useful, since shape functions cannot be effectively created when several nodes in a given region exist in a straight line (see section 2.1). To avoid poor node placement, we create a tetrahedral mesh automatically with Ansys and record node locations before discarding element information. This method ensures that we get a roughly even distribution of nodes.

Integration in our algorithm is done over a regular background mesh of varying density as shown in Fig.3. This background mesh is initially much larger than the volume of interest but we reject any cell whose centre is outside the brain volume. For most interior regions, we use a cell with volume of 500mm^3 . On the boundary and around the tumor, a higher resolution is needed to deal with irregular geometry and/or higher density of nodes. In these areas the volume of the cells drops to 125mm^3 . All cells are under-integrated (single Gauss point).

It is important to note that while our background cells appear to be standard hexahedral elements, they do not conform to boundaries. This would appear to give less accurate results, but we see in section 4 that this is not the case. Of course, if more accuracy was required then additional, smaller cells can be added and some large cells can be broken up to account for any geometry at any resolution. No consideration is needed when multiple small cells share a border with one large cell. All of this can be done automatically by an extremely simple code.

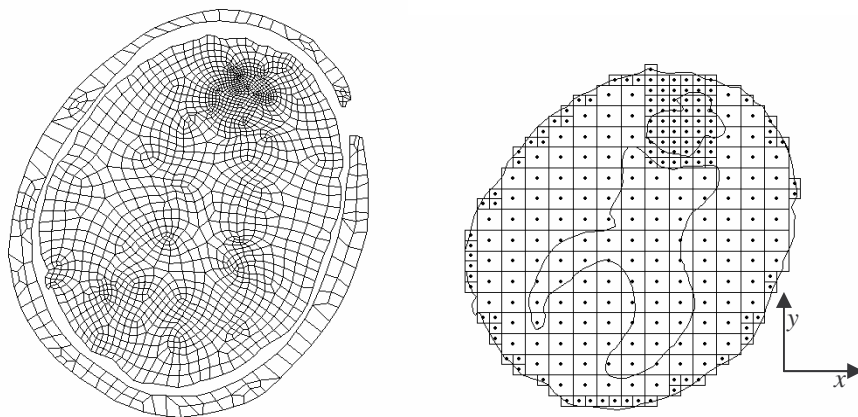


Fig. 3. Left: Hexahedral element mesh needed for LS DYNA simulation. Right: Background mesh used in our algorithm. The dot in the centre of each cell is the single integration point. Note that in our algorithm, the skull does not have a background mesh.

3.3 Loading and Boundary Condition

The brain, ventricles and tumor are modeled as having no gaps between parts. They are connected by sharing nodes along part boundaries. Between the brain and skull, there are many materials with complicated properties. For this study, it is sufficient to consider this subarachnoid space to be a gap of approximately 2-4mm between these two parts [3]. Appropriate contact surfaces are defined between the brain and skull with the assumption of no sliding friction.

We constrain all nodes in the direction normal to the slice to simulate the existence of the missing brain volume. During any neurosurgical procedure, the head would be totally anchored and the skull significantly stiffer than its contents. In both our simulations we treat the skull as a rigid and anchored body. In our algorithm this means that the skull only needs to be modeled along its contact region (interior surface). This explains why Fig. 3 does not show any background mesh for the skull.

We simulate external pressure on the brain (causing brain shift) by enforcing a displacement on nodes near the craniotomy as shown in Fig. 4. The displacement is enforced for 1s before removing the enforced displacement and allowing relaxation for 1s (total simulation time is 2s).

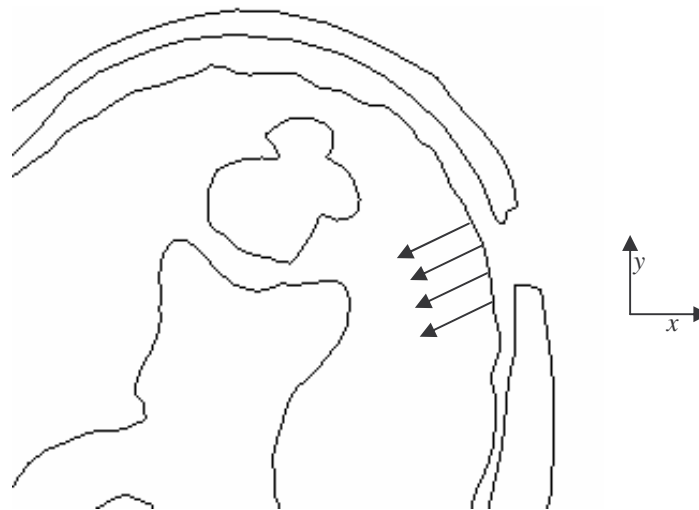


Fig. 4. Displacement is enforced on nodes near craniotomy.

4 Results

Table 1 shows the resulting displacement of the centre of mass for the brain, ventricles and tumor. We see that the relative displacement differences between the two algorithms are of the order 10^{-2} . Also, the absolute displacement differences are safely less than 0.85mm which is the resolution of the MRIs used in this study [17]. At this level of accuracy, it would now be more important (for this simulation) to refine the initial state than to refine the numerical algorithm.

Fig. 5 visually shows the high agreement between simulation results. Outlines from both simulations are shown and line up almost perfectly. As would be expected, the greatest difference is visible (as a slightly thicker outline) at the contact region where the two algorithms differ slightly. We should also be aware that slightly different nodal discretisations of the part boundaries give us a minor discrepancy which is not the fault of either algorithm. Note that it is the nodes, not the integration cells, that discretise the part boundaries.

Table 1. Coordinates of the centre of mass of the brain, ventricles and tumor. Coordinates in the z direction (normal to the slice) are not shown, since they are all 2.5mm and no differences are seen.

Part	Direction	Initial Coordinate (mm)	Displaced Coordinates		Relative Differences
			LS DYNA (mm)	Our algorithm (mm)	
Brain	x	13.3012	10.7133	10.7610	0.0184
	y	7.1770	3.9657	4.2143	0.0774
Ventricles	x	15.3711	12.4832	12.7567	0.0947
	y	-4.8039	-8.1255	-7.8064	0.0961
Tumor	x	34.4503	31.6203	31.8396	0.0775
	y	57.732	54.8762	55.0402	0.0574

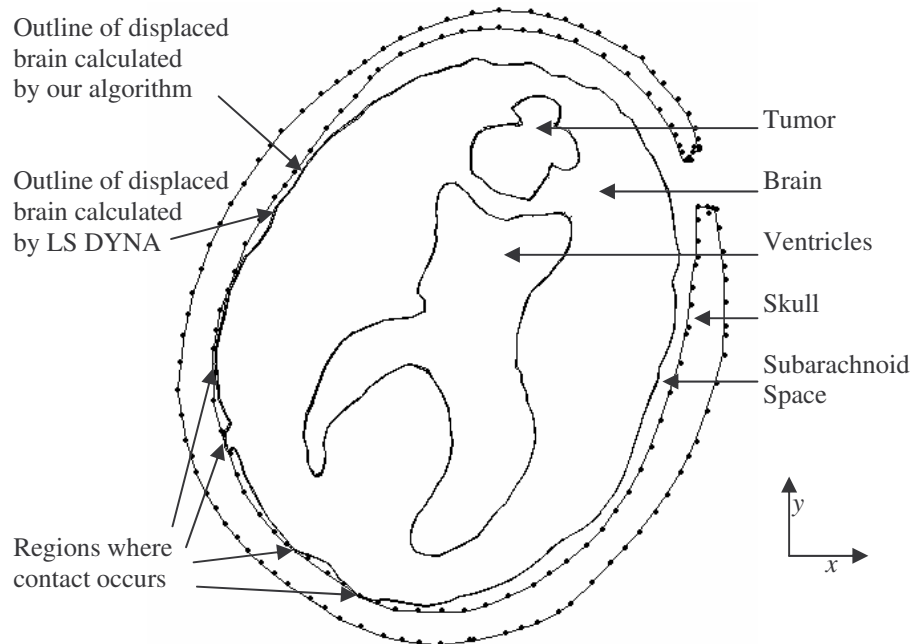


Fig. 5. Outlines of the displaced brain, ventricles and tumor from both simulations are displayed here on the same image to show the similarity of results. A greater difference in results is visible near the contact edges. The dots around the skull are reference markers, to ensure that the images are aligned correctly.

5 Conclusions

We have proposed an algorithm using EFG shape functions, integration over a regular background mesh of varying density, almost arbitrarily placed nodes, TL explicit dynamics formulation and nonlinear material models for the purpose of modeling surgical procedures. For validation purposes we gave a neurosurgical example of craniotomy induced brain shift and ran a parallel simulation with LS DYNA's established EFG solver.

By comparing displacements calculated by LS DYNA and our algorithm, we found the relative differences to be very small. Absolute displacement differences were less than 0.85 mm which is MRI voxel size. Thus the accuracy offered by our algorithm is sufficient for use in computer integrated surgery.

A major advantage of meshless methods such as EFG is their ability to easily discretise irregular geometries. This is why we feel that this step away from LS

DYNA's solver (which requires a boundary conforming, structured hexahedral element mesh for background integration) is a necessary one.

Ultimately, we intend to use EFG (and other meshless methods) coupled with FEA to provide more efficient methods in terms of both geometry discretisation and calculation time. This paper shows us that the TL explicit dynamics approach with almost arbitrarily placed nodes and regular background integration, is worth developing in the future for computer integrated surgery.

Acknowledgments. The financial support of the Australian Research Council is gratefully acknowledged, Grant No. DP0664534. MRIs were obtained by Brigham and Women's Hospital, Surgical Planning Laboratory in the course of research funded by NIH grants R21 MH67054, R01 LM007861 and P41 RR13218.

References

1. Cotin, S., H. Delingette, and N. Ayache, *Real-Time Elastic Deformations of Soft Tissues for Surgery Simulation*. IEEE Transactions on Visualization and Computer Graphics, 1999. 5(1): p. 62-73.
2. Bathe, K.-J., *Finite Element Procedures*. 1996: Prentice-Hall.
3. Wittek, A., et al., *Patient-Specific Model of Brain Deformation: Application to Medical Image Registration*. Journal of Biomechanics, Accepted 2006.
4. Wittek, A., et al. *Brain shift computation using a fully nonlinear biomechanical model*. in *8th International Conference on Medical Image Computing and Computer Assisted Surgery MICCAI 2005*. 2005. Palm Springs, California, USA: Springer-Verlag New York Inc.
5. Miller, K., et al., *Total Lagrangian Explicit Dynamics Finite Element Algorithm for Computing Soft Tissue Deformation*. Communications in Numerical Methods in Engineering, Accepted 2006.
6. Horton, A., A. Wittek, and K. Miller. *Computer Simulation of Brain Shift Using an Element Free Galerkin Method*. in *7th International Symposium on Computer Methods in Biomechanics and Biomedical Engineering*. 2006. Antibes, Cote d'Azur, France.
7. Belytschko, T., Y.Y. Lu, and L. Gu, *Element-free Galerkin methods*. International Journal for Numerical Methods in Engineering, 1994. 37: p. pp. 229-256.
8. Li, S. and W.K. Liu, *Meshfree Particle Methods*. 2004, New York: Springer.
9. LSTC, *LS-DYNA Keyword User's Manual*. 2003(Version 970).
10. Lancaster, P. and K. Salkauskas, *Surfaces generated by moving least squares methods*. Mathematics of Computation, 1992. 37: p. 141-158.
11. Miller, K., et al., *Total Lagrangian Explicit Dynamics Finite Element Algorithm for Computing Soft Tissue Deformation*. Communications in Numerical Methods in Engineering, 2006(Accepted May 2006, Available at <http://www3.interscience.wiley.com/>).
12. Mooney, M., *A theory of large elastic deformation*. Journal of Applied Physics, 1940. 11: p. 582-592.
13. Miller, K., *Biomechanics of Brain for Computer Integrated Surgery*. 2002, Warsaw: Publishing House of Warsaw University of Technology.
14. Miller, K. and K. Chinzei, *Mechanical properties of brain tissue in tension*. Journal of Biomechanics, 2002. 35: p. 483-490.
15. 3DSlicer, *Medical visualization and processing environment for research*, <http://www.slicer.org>, 2004.
16. Ansys, *Ansys LS-DYNA 9.0*. <http://www.ansys.com/>, 2004.
17. Bourgeois, G., et al., *Accuracy of MRI-guided stereotactic thalamic functional neurosurgery*. NEURORADIOLOGY, 1999. 41(9): p. 636-645.